Editors' Suggestion Featured in Physics

Observation of Interaction-Induced Mobility Edge in an Atomic Aubry-André Wire

Yunfei Wang,[1] Jia-Hui Zhang,[1] Yuqing Li,[1,2,*] Jizhou Wu,[1,2] Wenliang Liu,[1,2] Feng Mei,[1,2,†] Ying Hu,[1,2,‡] Liantuan Xiao,[1,2] Jie Ma,[1,2,§] Cheng Chin,[3] and Suotang Jia[1,2]

[1]*State Key Laboratory of Quantum Optics and Quantum Optics Devices, Institute of Laser Spectroscopy, Shanxi University, Taiyuan 030006, China*

[2]*Collaborative Innovation Center of Extreme Optics, Shanxi University, Taiyuan, Shanxi 030006, China*

[3]*James Franck Institute, Enrico Fermi Institute, Department of Physics, University of Chicago, Illinois 60637, USA*

(Received 26 April 2022; accepted 11 July 2022; published 1 September 2022)

A mobility edge, a critical energy separating localized and extended excitations, is a key concept for understanding quantum localization. The Aubry-André (AA) model, a paradigm for exploring quantum localization, does not naturally allow mobility edges due to self-duality. Using the momentum-state lattice of quantum gas of Cs atoms to synthesize a nonlinear AA model, we provide experimental evidence for a mobility edge induced by interactions. By identifying the extended-to-localized transition of different energy eigenstates, we construct a mobility-edge phase diagram. The location of a mobility edge in the low- or high-energy region is tunable via repulsive or attractive interactions. Our observation is in good agreement with the theory and supports an interpretation of such interaction-induced mobility edge via a generalized AA model. Our Letter also offers new possibilities to engineer quantum transport and phase transitions in disordered systems.

DOI: 10.1103/PhysRevLett.129.103401

Introduction.—The concept of a mobility edge (ME), a critical energy separating extended and exponentially localized energy eigenstates in the excitation spectrum, is key for understanding Anderson localization [1–13] induced by the random disorders in three dimensions [14]. In low dimensions, arbitrarily weak random disorders can make all single-particle eigenstates localize, hence the ME is absent. The localization phenomena have also been actively studied in the quasiperiodic lattice systems with incommensurate modulations [15–24], such as those described by the Aubry-André (AA) model [15].

Realization of the AA model in cold atoms has led to the first observation of the localization transition of a noninteracting Bose-Einstein condensate (BEC) [25]. As the AA model has self-dual symmetry [15], the localization transition is energy independent (i.e., no ME), with all eigenstates being localized across a single critical point. Intriguingly, variants of the AA model with broken self-duality, such as the generalized Aubry-André (GAA) model [26], can host a ME already in one dimension. So far, the existence of MEs has been mainly conjectured in noninteracting quasiperiodic lattice systems [26–35] and experimentally confirmed with cold atoms in optical lattices [36].

Beyond noninteracting systems, the realization and control of MEs are of fundamental interest, but are generally challenging. Recently, some atomic experiments in this direction have been carried out, showing how single-particle MEs are affected by weak interactions [37,38], and many-body MEs have been discussed in the context of the many-body localization [39]. In these experiments, however, a ME is already expected without interactions. It is thus highly desired to understand MEs based on systems with tunable interactions.

In this Letter, we demonstrate that a ME can be *induced* and *tuned* by interaction; the physical picture is shown in Fig. 1(a): weak interaction can have different dressing effects on different energy eigenstates of the AA model, resulting in a suppressed or enhanced localization of an eigenstate, thus a critical energy (i.e., ME) is expected in the excitation spectrum.

Experimentally, we observe signatures of MEs based on the momentum-state lattice of quasi-1D ^{133}Cs BEC that simulates a nonlinear AA model [Fig. 1(b)]. Exploiting the tunable scattering length of Cs atoms with Feshbach resonances [40–44], we realize a nonlinear AA model under a wide range of interactions and observe the extended-to-localized transitions that depend on the energy of the excited states. In particular, the controllability of all the system parameters including interactions allows us to access the highest excited state, which can be viewed as the ground state of the associated *negative* Hamiltonian. We demonstrate that interactions can enhance the localization of either low- or high-energy eigenstates, depending on the sign of the interactions. We further construct a mobility-edge phase diagram, which agrees well with the theory.

Such interaction-induced ME can be understood through an effective noninteracting GAA model. While the nonlinear AA model and its variants [45–48] have been studied

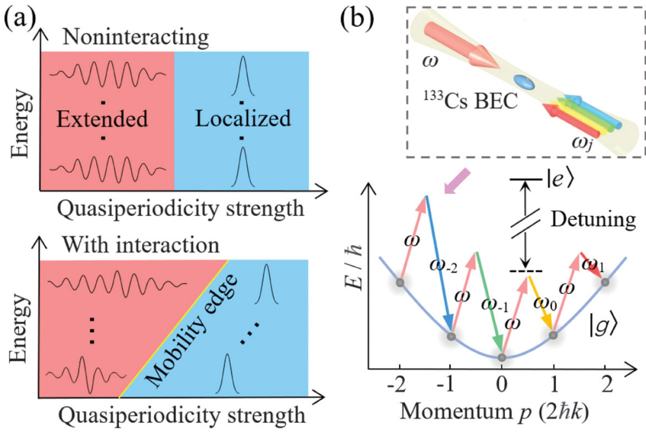

FIG. 1. Illustration of interaction-induced mobility edge and experimental scheme. (a) Top: without interaction, all eigenstates in the energy spectrum are either localized (blue) or extended (red). Bottom: weak interaction can suppress or enhance localization depending on the energy, thus a mobility edge emerges in the spectrum. (b) Top: a quasi-1D ^{133}Cs BEC with tunable atomic interaction is illuminated by a pair of counterpropagating laser beams, one with a frequency ω and the other with multifrequency components ω_j ($j = -10, \ldots, 9$). Bottom: the lasers, far detuned from the atomic transition, drive a series of engineered two-photon Bragg transitions that couple 21 momentum states with the increment of $2\hbar k$ (with $k = 2\pi/\lambda$). This synthesizes a nonlinear AA model with $L = 21$ sites in the momentum space.

before in optical and atomic setups [6,8,45–51], the exploration of MEs in the model remains elusive.

ME in the nonlinear AA model.—We start by theoretically showing how a ME arises in the nonlinear AA model,

$$\begin{aligned} i\hbar\dot{\varphi}_j = {} & J(\varphi_{j+1} + \varphi_{j-1}) \\ & + \Delta\cos(2\pi\beta j + \phi)\varphi_j - U|\varphi_j|^2\varphi_j. \end{aligned} \tag{1}$$

Here $\hbar$ is the reduced Planck's constant, φ_j is the wave function at site j in a lattice of size L with $\sum_j |\varphi_j|^2 = 1$, and J is the nearest-neighbor coupling. The quasiperiodic lattice potential with $\beta = (\sqrt{5} - 1)/2$ has a modulation strength Δ and phase ϕ. The nonlinear term characterized by U in our subsequent discussion arises from the atomic interaction. When $U = 0$, Eq. (1) reduces to the AA model, with all eigenstates being extended for $\Delta/J < 2$ and localized for $\Delta/J > 2$.

We are interested in the weak interaction regime $|U/J| \lesssim 1$ where the self-trapping [52,53] does not occur, and every eigenstate has a correspondence in the noninteracting counterpart [54]. Insights can be obtained by noting that the combination of the nonlinear term and the incommensurate modulation results in a density-dependent potential $V_j^{\rm ext} = \Delta\cos(2\pi\beta j + \phi) - Un_j$, with the density $n_j = |\varphi_j|^2$. As the density distribution is shaped by the incommensurate modulation, $V_j^{\rm ext}$ contains *multiple* harmonics of the quasiperiodicity (i.e., $2\pi\beta$), which breaks the self-duality and leads to a ME. For $|U/\Delta| \ll 1$, perturbative analysis suggests $V_j^{\rm ext}$ is effectively a GAA lattice potential. For instance, when $\phi = 0$, by Fourier expanding the density up to the second harmonics of the quasiperiodicity, we have $V_j^{\rm ext} \approx (\Delta - Uc_1)\cos(2\pi\beta j) - Uc_2\cos(4\pi\beta j)$ (apart from some constant), with the expansion coefficients c_1 and c_2. It approximates the GAA lattice potential [26]

$$V_{\rm GAA}^j = \Delta\frac{\cos(2\pi\beta j)}{1 - \alpha^*(U)\cos(2\pi\beta j)}, \tag{2}$$

with $\alpha^* \ll 1$ and $\alpha^* \propto -U$, up to the second harmonics. Thus, the physics of Eq. (1) may be understood via an "effective noninteracting GAA model": $i\hbar\dot{\varphi}_j = J(\varphi_{j+1} + \varphi_{j-1}) + V_{\rm GAA}^j\varphi_j$. As the GAA model hosts an exact ME [26], the location E_c of ME in a weakly nonlinear AA model is expected to be

$$E_c = \frac{\mathrm{sgn}(\Delta)(2|J| - |\Delta|)}{\alpha^*(U)}, \tag{3}$$

where sgn denotes the sign function. Because $\alpha^* \propto -U$, we expect the location of ME in the low- or high-energy region is swapped when $U \to -U$.

The above analysis is supported by numerical calculations. We focus on the ground state (GS) and the highest excited state (ES) of the nonlinear AA model [55] and characterize their degree of localization via the participation ratio

$$r = \frac{1}{L}\frac{1}{\sum_{j=1}^{L} n_j^2}. \tag{4}$$

For a localized state, $r \approx 0$; for an extended state, the maximum possible r is 1. Figures 2(a) and 2(b) show the participation ratio r as a function of Δ/J and U/J for the GS and ES, respectively. To identify the transition from the extended to the localized, we use the critical value of r at $\Delta/J = 2$ in the noninteracting limit (see white curves) [56]; for $L = 21$ sites, the critical value is $r = 0.103$. We see that, whereas the transition points of the GS and ES coincide without interaction, they differ in the presence of interaction, suggesting the transition is energy dependent. Moreover, adding $U > 0$ enhances localization of the GS but delocalizes the ES, whereas the opposite occurs for $U < 0$. This can be intuitively understood, because for $U > 0$ ($U < 0$), a more localized (extended) GS is favored to minimize the interaction energy $-Un_j$; whereas the opposite is expected for the ES, which may be viewed as the GS of the negative Hamiltonian.

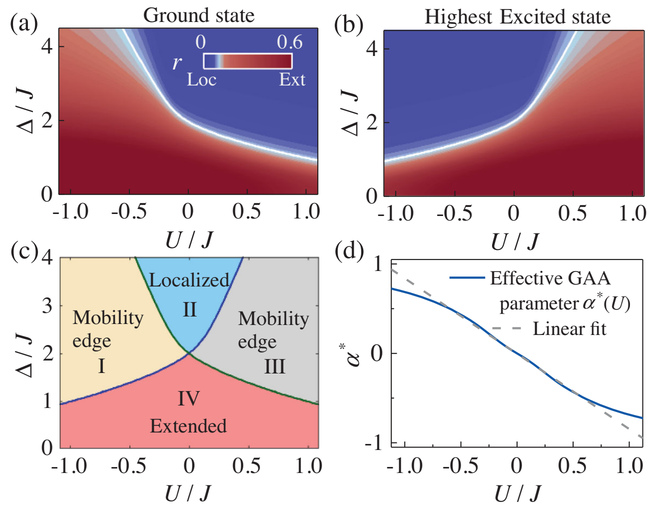

FIG. 2. Theoretical prediction. (a), (b) Participation ratio r of the (a) GS and (b) ES for various quasiperiodic modulation strengths Δ/J and interactions U/J. The state is localized (extended) in the blue (red) region. The transition (white curve) is identified as where $r = 0.103$, the critical value in the noninteracting case [56]. (c) Regimes in the parameter spaces $(\Delta/J, U/J)$ where a ME may exist. In phases I and III, extended and localized eigenstates coexist, signaling a ME; in phase I (III), low-energy states are extended (localized). The boundaries are denoted by the green and blue curves. (d) Verification of the effective GAA model. The α^* defined in Eq. (3) is calculated as a function of U/J (solid curve). For small U/J, it exhibits a linear relation $\alpha^* = -0.81U/J$ (dashed curve). In all panels, the lattice size is $L = 21$.

The critical points of the GS and ES divide the parameter space (Δ, U) into four regimes [Fig. 2(c)]. In phase II (IV), all states are localized (extended). However, in both phases I and III, extended and localized states coexist, signaling the existence of ME. When increasing the incommensurate modulation strength Δ, the ME emerges from the high-energy regime in I ($U < 0$), while it emerges from the low-energy regime in III ($U > 0$).

We validate the effective GAA model through numerical simulations. We calculate the effective parameter $\alpha^* = (\Delta_c^g - \Delta_c^e)/(E_e^c - E_g^c)$ based on Eq. (3), where E_g^c (E_e^c) denotes the energy of the GS (ES) at the critical point Δ_c^g (Δ_c^e), representing where the ME coincides with the lowest (highest) energy. Figure 2(d) shows α^* as a function of U/J (blue curve). It is linear for small interactions, confirming the previous conjecture. In the linear regime, we expect the location of the ME to be given by Eq. (3). When the linearity breaks down, the effective model is no longer suitable.

Experimental realization of the model.—We experimentally realize the nonlinear AA model using the momentum-state lattice of ^{133}Cs BEC that contains 4×10^4 atoms in the hyperfine state $|F = 3, m_F = 3\rangle$ [Fig. 1(b)] [57]. We start with a BEC confined in a quasi-1D optical trap (see Supplemental Material [58]). Two counterpropagating laser beams with the wavelength $\lambda = 1064$ nm are applied, one with a frequency ω, while the other contains multifrequency components $\omega_j = \omega - \Delta\omega_j$, $j = -10, \ldots, 9$. They drive a series of two-photon Bragg transitions to couple 21 discrete momentum states with the momentum increment of $2\hbar k$ (with $k = 2\pi/\lambda$), which simulates the AA model of $L = 21$ sites with the nearest-neighbor coupling J [59]. The incommensurate modulation is realized by engineering $\Delta\omega_j$ to yield an on-site energy $\Delta\cos(2\beta\pi j + \phi)$ [58] with both Δ and ϕ controllable via Bragg lasers. We employ a broad Feshbach resonance centered at magnetic field $B = -11.7$ G to tune the atomic s-wave scattering length [40–44]. According to the mean-field theory of the momentum lattice system [38,60–62], the atomic interaction leads to the nonlinear term in Eq. (1), with $U = (4\pi\hbar^2 a/m)\bar{\rho}$, where m is the atomic mass and $\bar{\rho}$ is an effective atomic density [58]. We note that a quasi-1D BEC can be stable for $a < 0$ [63]; experimentally, we do not observe the collapse of BEC for $a < 0$ on the timescale of 2 ms relevant for our measurements. To avoid significant three-body loss [64], we restrict ourselves to $a > -100a_0$ (a_0 is the Bohr radius).

To confirm the realization of the nonlinear AA model, we first tune $a \approx 0$ and observe the transport of the noninteracting BEC by controlling the incommensurate modulation strength Δ. Initially, the BEC with zero momentum is prepared at momentum-state lattice site $j = 0$, before the Bragg lasers are switched on. After an evolution time t, the momentum distribution is measured through the time-of-flight (TOF) technique [58]. TOF images for $t = 4\hbar/J = 1.28$ ms under different Δ/J are illustrated in Fig. 3(a). As expected from the AA model, atoms spread over several lattice sites for $\Delta/J < 2$, but localize sharply near the initial position for $\Delta/J > 2$. Figure 3(b) shows the time-dependent momentum width $\langle d(t)\rangle = \sum_j |j| n_j(t)$, where $n_j(t)$ is the measured fraction of atomic population at the momentum state $|2j\hbar k\rangle$ at time t. We observe the familiar crossover from the ballistic transport to localization with increasing Δ/J, in agreement with the numerical simulations (solid lines) based on the Gross-Pitaevskii (GP) equation (see Supplemental Material [58]).

Next, we tune the scattering length from $a < 0$ to $a > 0$ using the broad Feshbach resonance and fix the incommensurate modulation strength at $\Delta/J = 1$. Figure 3(c) shows the measured momentum width $\langle d\rangle$ at $t = 2\hbar/J = 0.64$ ms under various interactions. We observe $\langle d\rangle$ decreases with the interaction strength, regardless of its sign, suggesting an increased degree of localization. The experiment agrees qualitatively with the GP calculations [58] (red curve). Note that, for $a < 0$, the discrepancy between the experiment and theory is likely caused by the nonadiabatic effects in the Feshbach tuning, which generate

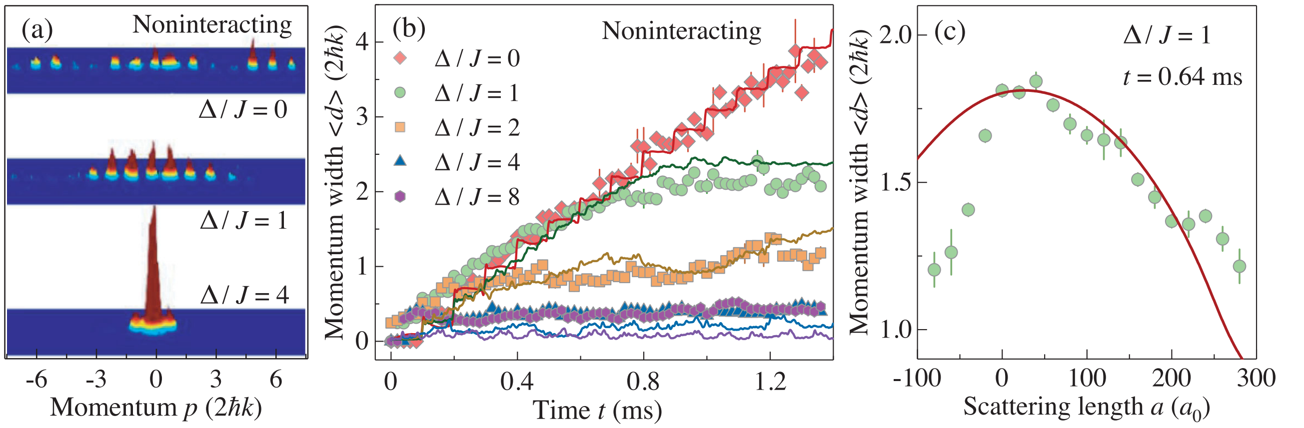

FIG. 3. Experimental realization of the nonlinear AA model in a Cs BEC with tunable quasiperiodic modulation strength Δ/J and interaction U/J. (a) Images of momentum distribution for various Δ/J in a noninteracting BEC. The Δ/J is tuned via engineering the frequency difference between the pair of Bragg lasers in Fig. 1(b). The BEC is initialized at the momentum lattice site $j = 0$. The absorption image is taken after $t = 1.28$ ms evolution and 18 ms TOF. (b) Measured momentum width $\langle d(t)\rangle$ as a function of the evolution time t in a noninteracting BEC under various Δ/J. Corresponding solid curves denote the numerical simulations (see Supplemental Material [58]). (c) Measured momentum width $\langle d\rangle$ at $t = 0.64$ ms as a function of the scattering length a (in units of Bohr radius a_0) for $\Delta/J = 1$. The scattering length is tuned via a Feshbach resonance. The solid curve denotes the numerical simulation [58]. Error bars denote 1σ standard deviations. In all panels, the coupling rates are $J/\hbar = 2\pi \times 500$ Hz.

thermal atoms reducing the coupling efficiency in the Bragg transitions.

Construction of ME phase diagram.—Important for our Letter is the preparation of the GS and ES under various incommensurate modulation strengths and interactions. We prepare the GS following the adiabatic protocol in Ref. [38]. It consists of switching off the laser coupling between lattice sites and initializing atoms in the ground state at zero-momentum site $j = 0$. Then, by linearly ramping the coupling from $J = 0$ to $J/\hbar = 2\pi \times 275$ Hz in 1 ms and holding there for 1 ms, the initial state is transferred to the GS of the lattice system.

A reliable preparation of the ES, however, was nontrivial due to nonadiabatic effects [38]. Here we adopt a strategy that is motivated by the fact that the ES of a Hamiltonian H can be viewed as the GS of $-H$. Experimentally, in preparing the ES of a system with desired J, Δ, and a, we instead realize an associated "negative Hamiltonian" (i.e., $-H$) with $-J$, $-\Delta$, and $-a$. To realize $-J$, we introduce a relative phase π in the two-photon Bragg transition coupling neighboring momentum states [cf. Fig. 1(b)]. The $-\Delta$ is achieved by tuning ϕ. Crucially, the conversion from a to $-a$ is uniquely enabled by Feshbach tuning of the interaction of Cs atoms. Then we adiabatically prepare the GS of the negative system similar to before: after switching off the laser coupling and initializing atoms at a site with the lowest energy, we linearly ramp up J, thus achieving the ES of the original system.

After the state preparation, we measure the population in each momentum mode to obtain the participation ratio r according to Eq. (4). We identify the potential extended-to-localized transition by numerically fitting the experimental data of r as a function of Δ/J [58], as shown in Figs. 4(a) and 4(b). For $U \approx 0$, the transition is at $\Delta/J = 2$ for both the GS and ES, as expected. Comparing Figs. 4(a) and 4(b) shows that the localization of the GS is enhanced (suppressed) under $U > 0$ ($U < 0$), whereas the opposite occurs for the ES, in agreement with the predictions. Owing to the nonadiabatic effect in the experimental ramp, the participation ratio r is generically smaller than the idealized value expected from Eq. (1) [58]. Moreover, the experimental r deep in the localized phase is slightly higher than $r = 1/21$ [58] due to the residual population. Nevertheless, these imperfections and finite-size effect do not qualitatively change the transitions.

Finally, to construct the phase diagram, we collect the extracted transition points of the GS and ES under various interactions into Fig. 4(c). The good agreement between the experiment and theory provides strong evidence of the existence of interaction-induced ME. It also confirms that, depending on whether the atomic interaction U is attractive or repulsive, the ME emerges from the high- or low-energy region of the excitation spectrum. In the inset of Fig. 4(c), we compare the experimental data with the predictions from the effective GAA model [cf. Fig. 2(d)]. As shown, the effective model provides a good explanation of the data for $|U/J| \lesssim 0.25$, suggesting the location of the ME in this regime is given by Eq. (3).

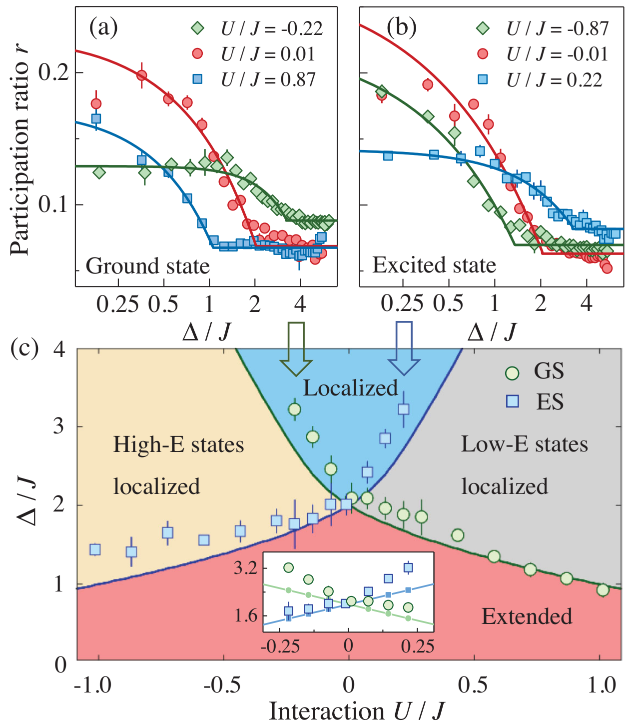

FIG. 4. Construction of ME phase diagram. (a),(b) Identification of the extended-to-localized transition points of the (a) GS and (b) ES. The experimental participation ratio r is shown as a function of quasiperiodic modulation Δ/J in the semilog$_2$ plot for various interactions. By fitting (solid curves) the experimental data via an empirical relation [58], we extract the transition point. In (a) and (b), the error bar indicates the 1σ standard deviation. (c) Construction of the phase diagram and identification of ME. We superimpose the extracted transition points of the GS (green circles) and ES (blue squares) on the theoretical phase diagram in Fig. 2(c). Inset: we compare the data for $|U/J| < 0.25$ with the predictions from the effective GAA model [green (blue) line for the GS (ES)]. The error bar in (c) shows the fitting error. In (a)–(c), the coupling rates are $J/\hbar = 2\pi \times 275$ Hz.

Conclusion.—In this Letter, we have provided experimental evidence that a ME can be induced and controlled by interactions in a 1D quasiperiodic momentum lattice. Our observations may further understandings of the ME in an interacting system and offer intriguing insights into the interplay between disorder and interaction [65–67]. Moreover, the widely tunable atomic interaction featured by the Cs atoms presents new opportunities for the quantum transport and quantum phase transitions in disordered systems.

We acknowledge helpful discussions with Biao Wu, Xiaopeng Li, Zhihao Xu, and Shuai Chen. This research is funded by the National Key Research and Development Program of China (Grant No. 2017YFA0304203), National Natural Science Foundation of China (Grants No. 62020106014, No. 92165106, No. 62175140, No. 12104276, No. 11874038, No. 12034012, and No. 12074234). C. C. acknowledges support by the National Science Foundation (Grant No. PHY-2103542).

*lyqing.2006@163.com
†meifeng@sxu.edu.cn
‡huying@sxu.edu.cn
§mj@sxu.edu.cn

[1] P. W. Anderson, Absence of diffusion in certain random lattices, Phys. Rev. **109**, 1492 (1958).
[2] R. Dalichaouch, J. P. Armstrong, S. Schultz, P. M. Platzman, and S. L. McCall, Microwave localization by two-dimensional random scattering, Nature (London) **354**, 53 (1991).
[3] D. Wiersma, P. Bartolini, A. Lagendijk, and R. Righini, Localization of light in a disordered medium, Nature (London) **390**, 671 (1997).
[4] A. A. Chabanov, M. Stoytchev, and A. Z. Genack, Statistical signatures of photon localization, Nature (London) **404**, 850 (2000).
[5] M. Störzer, P. Gross, C. Aegerter, and G. Maret, Observation of the Critical Regime near Anderson Localization of Light, Phys. Rev. Lett. **96**, 063904 (2006).
[6] T. Schwartz, G. Bartal, S. Fishman, and M. Segev, Transport and Anderson localization in disordered two-dimensional photonic lattices, Nature (London) **446**, 52 (2007).
[7] J. Chabé, G. Lemarié, B. Grémaud, D. Delande, P. Szriftgiser, and J. C. Garreau, Experimental Observation of the Anderson Metal-Insulator Transition with Atomic Matter Waves, Phys. Rev. Lett. **101**, 255702 (2008).
[8] Y. Lahini, A. Avidan, F. Pozzi, M. Sorel, R. Morandotti, D. Christodoulides, and Y. Silberberg, Anderson Localization and Nonlinearity in One-Dimensional Disordered Photonic Lattices, Phys. Rev. Lett. **100**, 013906 (2008).
[9] J. Billy, V. Josse, Z. C. Zuo, A. Bernard, B. Hambrecht, P. Lugan, D. Clément, L. Sanchez-Palencia, P. Bouyer, and A. Aspect, Direct observation of Anderson localization of matter waves in a controlled disorder, Nature (London) **453**, 891 (2008).
[10] S. S. Kondov, W. R. McGehee, J. J. Zirbel, and B. DeMarco, Three-dimensional Anderson localization of ultracold matter, Science **334**, 66 (2011).
[11] F. Jendrzejewski, A. Bernard, K. Müller, P. Cheinet, V. Josse, M. Piraud, L. Pezzé, L. Sanchez-Palencia, A. Aspect, and P. Bouyer, Three-dimensional localization of ultracold atoms in an optical disordered potential, Nat. Phys. **8**, 398 (2012).
[12] I. Manai, J. Clément, R. Chicireanu, C. Hainaut, J. C. Garreau, P. Szriftgiser, and D. Delande, Experimental Observation of Two-Dimensional Anderson Localization with the Atomic Kicked Rotor, Phys. Rev. Lett. **115**, 240603 (2015).
[13] D. White, T. Haase, D. Brown, M. Hoogerland, M. Najafabadi, J. Helm, C. Gies, D. Schumayer, and D. W. Hutchinson, Observation of two-dimensional Anderson localisation of ultracold atoms, Nat. Commun. **11**, 4942 (2020).

[14] E. Abrahams, P. W. Anderson, D. C. Licciardello, and T. V. Ramakrishnan, Scaling Theory of Localization: Absence of Quantum Diffusion in Two Dimensions, Phys. Rev. Lett. **42**, 673 (1979).

[15] S. Aubry and G. André, Analyticity breaking and Anderson localization in incommensurate lattices, Ann. Isr. Phys. Soc. **3**, 18 (1980).

[16] D. R. Grempel, S. Fishman, and R. E. Prange, Localization in an Incommensurate Potential: An Exactly Solvable Model, Phys. Rev. Lett. **49**, 833 (1982).

[17] M. Kohmoto, L. Kadanoff, and C. Tang, Localization Problem in One Dimension: Mapping and Escape, Phys. Rev. Lett. **50**, 1870 (1983).

[18] M. Kohmoto, Metal-Insulator Transition and Scaling for Incommensurate Systems, Phys. Rev. Lett. **51**, 1198 (1983).

[19] S. D. Sarma, A. Kobayashi, and R. E. Prange, Proposed Experimental Realization of Anderson Localization in Random and Incommensurate Artificially Layered Systems, Phys. Rev. Lett. **56**, 1280 (1986).

[20] D. J. Thouless, Localization by a Potential with Slowly Varying Period, Phys. Rev. Lett. **61**, 2141 (1988).

[21] M. Modugno, Exponential localization in one-dimensional quasi-periodic optical lattices, New J. Phys. **11**, 033023 (2009).

[22] J. Biddle, B. Wang, D. J. Priour, Jr., and S. D. Sarma, Localization in one-dimensional incommensurate lattices beyond the Aubry-André model, Phys. Rev. A **80**, 021603 (R) (2009).

[23] J. Biddle, D. J. Priour, Jr., B. Wang, and S. D. Sarma, Localization in one-dimensional lattices with non-nearest-neighbor hopping: Generalized Anderson and Aubry-André models, Phys. Rev. B **83**, 075105 (2011).

[24] T. Xiao, D. Z. Xie, Z. L. Dong, T. Chen, W. Yi, and B. Yan, Observation of topological phase with critical localization in a quasi-periodic lattice, Sci. Bull. **66**, 2175 (2021).

[25] G. Roati, C. D'Errico, L. Fallani, M. Fattori, C. Fort, M. Zaccanti, G. Modugno, M. Modugno, and M. Inguscio, Anderson localization of a non-interacting Bose-Einstein condensate, Nature (London) **453**, 895 (2008).

[26] S. Ganeshan, J. H. Pixley, and S. D. Sarma, Nearest Neighbor Tight Binding Models with an Exact Mobility Edge in One Dimension, Phys. Rev. Lett. **114**, 146601 (2015).

[27] S. D. Sarma, S. He, and X. C. Xie, Mobility Edge in a Model One-Dimensional Potential, Phys. Rev. Lett. **61**, 2144 (1988).

[28] D. J. Boers, B. Goedeke, D. Hinrichs, and M. Holthaus, Mobility edges in bichromatic optical lattices, Phys. Rev. A **75**, 063404 (2007).

[29] J. Biddle and S. D. Sarma, Predicted Mobility Edges in One-Dimensional Incommensurate Optical Lattices: An Exactly Solvable Model of Anderson Localization, Phys. Rev. Lett. **104**, 070601 (2010).

[30] X. Li, X. P. Li, and S. D. Sarma, Mobility edges in one-dimensional bichromatic incommensurate potentials, Phys. Rev. B **96**, 085119 (2017).

[31] H. P. Yao, A. Khoudli, L. Bresque, and L. Sanchez-Palencia, Critical Behavior and Fractality in Shallow One-Dimensional Quasiperiodic Potentials, Phys. Rev. Lett. **123**, 070405 (2019).

[32] X. Deng, S. Ray, S. Sinha, G. V. Shlyapnikov, and L. Santos, One-Dimensional Quasicrystals with Power-Law Hopping, Phys. Rev. Lett. **123**, 025301 (2019).

[33] X. Li and S. D. Sarma, Mobility edge and intermediate phase in one-dimensional incommensurate lattice potentials, Phys. Rev. B **101**, 064203 (2020).

[34] Y. C. Wang, X. Xia, L. Zhang, H. P. Yao, S. Chen, J. G. You, Q. Zhou, and X. J. Liu, One-Dimensional Quasiperiodic Mosaic Lattice with Exact Mobility Edges, Phys. Rev. Lett. **125**, 196604 (2020).

[35] S. Roy, T. Mishra, B. Tanatar, and S. Basu, Reentrant Localization Transition in a Quasiperiodic Chain, Phys. Rev. Lett. **126**, 106803 (2021).

[36] H. Lüschen, S. Scherg, T. Kohlert, M. Schreiber, P. Bordia, X. Li, S. D. Sarma, and I. Bloch, Single-Particle Mobility Edge in a One-Dimensional Quasiperiodic Optical Lattice, Phys. Rev. Lett. **120**, 160404 (2018).

[37] F. A. An, E. J. Meier, and B. Gadway, Engineering a Flux-Dependent Mobility Edge in Disordered Zigzag Chains, Phys. Rev. X **8**, 031045 (2018).

[38] F. A. An, K. Padavić, E. J. Meier, S. Hegde, S. Ganeshan, J. H. Pixley, S. Vishveshwara, and B. Gadway, Interactions and Mobility Edges: Observing the Generalized Aubry-André Model, Phys. Rev. Lett. **126**, 040603 (2021).

[39] T. Kohlert, S. Scherg, X. Li, H. Lüschen, S. D. Sarma, I. Bloch, and M. Aidelsburger, Observation of Many-Body Localization in a One-Dimensional System with a Single-Particle Mobility Edge, Phys. Rev. Lett. **122**, 170403 (2019).

[40] T. Weber, J. Herbig, M. Mark, H.-C. Nägerl, and R. Grimm, Bose-Einstein condensation of cesium, Science **299**, 232 (2003).

[41] T. Kraemer, J. Herbig, M. Mark, T. Weber, C. Chin, H.-C. Nägerl, and R. Grimm, Optimized production of a cesium Bose-Einstein condensate, Appl. Phys. B **79**, 1013 (2004).

[42] C. Chin, V. Vuletić, A. Kerman, S. Chu, E. Tiesinga, P. Leo, and C. Williams, Precision Feshbach spectroscopy of ultracold Cs_2, Phys. Rev. A **70**, 032701 (2004).

[43] C.-L. Hung, X. B. Zhang, N. Gemelke, and C. Chin, Accelerating evaporative cooling of atoms into Bose-Einstein condensation in optical traps, Phys. Rev. A **78**, 011604(R) (2008).

[44] C. Chin, R. Grimm, P. Julienne, and E. Tiesinga, Feshbach resonances in ultracold gases, Rev. Mod. Phys. **82**, 1225 (2010).

[45] Y. Lahini, R. Pugatch, F. Pozzi, M. Sorel, R. Morandotti, N. Davidson, and Y. Silberberg, Observation of a Localization Transition in Quasiperiodic Photonic Lattices, Phys. Rev. Lett. **103**, 013901 (2009).

[46] F. A. An, E. J. Meier, and B. Gadway, Diffusive and arrested transport of atoms under tailored disorder, Nat. Commun. **8**, 325 (2017).

[47] B. Deissler, M. Zaccanti, G. Roati, C. D'Errico, M. Fattori, M. Modugno, G. Modugno, and M. Inguscio, Delocalization of a disordered bosonic system by repulsive interactions, Nat. Phys. **6**, 354 (2010).

[48] E. Lucioni, B. Deissler, L. Tanzi, G. Roati, M. Zaccanti, M. Modugno, M. Larcher, F. Dalfovo, M. Inguscio, and G. Modugno, Observation of Subdiffusion in a Disordered Interacting System, Phys. Rev. Lett. **106**, 230403 (2011).

[49] M. J. McKenna, R. L. Stanley, and J. D. Maynard, Effects of Nonlinearity on Anderson Localization, Phys. Rev. Lett. **69**, 1807 (1992).

[50] A. S. Pikovsky and D. L. Shepelyansky, Destruction of Anderson Localization by a Weak Nonlinearity, Phys. Rev. Lett. **100**, 094101 (2008).

[51] S. Lellouch and L. Sanchez-Palencia, Localization transition in weakly interacting Bose superfluids in one-dimensional quasiperiodic lattices, Phys. Rev. A **90**, 061602 (R) (2014).

[52] A. Smerzi, S. Fantoni, S. Giovanazzi, and S. R. Shenoy, Quantum Coherent Atomic Tunneling between Two Trapped Bose-Einstein Condensates, Phys. Rev. Lett. **79**, 4950 (1997).

[53] M. Albiez, R. Gati, J. Fölling, S. Hunsmann, M. Cristiani, and M. Oberthaler, Direct Observation of Tunneling and Nonlinear Self-Trapping in a Single Bosonic Josephson Junction, Phys. Rev. Lett. **95**, 010402 (2005).

[54] B. Wu and Q. Niu, Superfluidity of Bose-Einstein condensate in an optical lattice: Landau-Zener tunnelling and dynamical instability, New J. Phys. **5**, 104 (2003).

[55] To numerically calculate the highest excited state, we invert the sign of all the system parameters in the nonlinear AA model and use imaginary time evolution to find its ground state.

[56] This provides a convenient way for numerically identifying the critical point when the system is small. It is consistent with the more generic approach using the empirical relation fitting to identify the transition, as we did later in the experiment.

[57] Y. F. Wang, Y. Q. Li, J. Z. Wu, W. L. Liu, J. Z. Hu, J. Ma, L. T. Xiao, and S. T. Jia, Hybrid evaporative cooling of ^{133}Cs atoms to Bose-Einstein condensation, Opt. Express **29**, 13960 (2021).

[58] See Supplemental Material at http://link.aps.org/supplemental/10.1103/PhysRevLett.129.103401 for details of our experiments, theoretical calculations, identification of transition points, and the analysis of imperfections such as nonadiabatic effects.

[59] E. J. Meier, F. A. An, and B. Gadway, Atom-optics simulator of lattice transport phenomena, Phys. Rev. A **93**, 051602(R) (2016).

[60] T. Chen, D. Z. Xie, B. Gadway, and B. Yan, A Gross-Pitaevskii-equation description of the momentum-state lattice: Roles of the trap and many-body interactions, arXiv:2103.14205v2.

[61] F. A. An, E. J. Meier, J. Ang'ong'a, and B. Gadway, Correlated Dynamics in a Synthetic Lattice of Momentum States, Phys. Rev. Lett. **120**, 040407 (2018).

[62] F. A. An, B. Sundar, J. P. Hou, X.-W. Luo, E. J. Meier, C. W. Zhang, K. R. A. Hazzard, and B. Gadway, Nonlinear Dynamics in a Synthetic Momentum-State Lattice, Phys. Rev. Lett. **127**, 130401 (2021).

[63] C. J. Pethick and H. Smith, *Bose-Einstein Condensation in Dilute Gases* (Cambridge University Press, Cambridge, England, 2008).

[64] T. Kraemer, M. Mark, P. Waldburger, J. G. Danzl, C. Chin, B. Engeser, A. D. Lange, K. Pilch, A. Jaakkola, H.-C. Nägerl, and R. Grimm, Evidence for Efimov quantum states in an ultracold gas of caesium atoms, Nature (London) **440**, 315 (2006).

[65] D. A. Abanin, E. Altman, I. Bloch, and M. Serbyn, Many-body localization, thermalization, and entanglement, Rev. Mod. Phys. **91**, 021001 (2019).

[66] D. L. Deng, S. Ganeshan, X. P. Li, R. Modak, S. Mukerjee, and J. H. Pixley, Many-body localization in incommensurate models with a mobility edge, Ann. Phys. (Amsterdam) **529**, 1600399 (2017).

[67] X. P. Li, S. Ganeshan, J. H. Pixley, and S. D. Sarma, Many-Body Localization and Quantum Nonergodicity in a Model with a Single-Particle Mobility Edge, Phys. Rev. Lett. **115**, 186601 (2015).